

Ramus: A Frequency-Multiplexed Power Bus for Powering, Sensing and Controlling Robots

Yuki Nishizawa, Takuya Sasatani, Matthew Ishige,
Yoshiaki Narusue, Takuya Umedachi, and Yoshihiro Kawahara

Abstract—As robots become more complex, small, and sophisticated, the cost and effort necessary for “wiring” become critical; the complex wiring makes the fabrication costly and necessitates care about space and stiffness of wires, which can inhibit the deformation of soft-bodied robots. The concept of power bus, which powers, controls, and monitors multiple slave modules (*e.g.*, actuators, sensors) via a shared bus is one countermeasure for this challenge. However, handling many slave modules in real-time remains an unsolved issue; prior work suffers from a delay corresponding to the number of slaves or requires a rich signal processing unit in each slave module, which makes them unsuitable for controlling numerous actuators. To address this issue, we propose a frequency-multiplexed power bus, which integrates bandpass filters and load-modulation communication; our method enables us to power, control, and monitor all slave modules at once via a single pair of wires. Through analysis and experiments, we showed that eight nodes can be accommodated within a 9 MHz frequency band and can be independently controlled; finally, a caterpillar-like robot with four sensors and actuators was successfully driven by Ramus.

I. INTRODUCTION

The advancement in actuating and sensing technology enabled the miniaturization of modules with actuating/sensing capability [1]; this advancement benefits emerging areas such as small-bodied robots, which need to integrate various functions into a small form-factor, and soft-bodied robots, which the massive degrees of freedom requires numerous controlled actuators for sophisticated control [2]. An emerging issue here is that as the number and density of these integrated modules increase, the cost and effort necessary for “wiring” these modules also increase. This makes quick prototyping difficult and inhibits deployment due to the decreased reliability, which derives from the numerous wires and connections. Moreover, the weight,

volume, and stiffness of these wires become troublesome in many cases; as for small robots (*e.g.*, insect-inspired robots [3]), non-trivial wiring space, as well as an extra payload, needs to be allocated; as for soft-bodied/flexible robots (*e.g.*, self-folding robots [4], bio-inspired robots [2]), the desired deformation can be easily inhibited by the non-ideal stiffness of these wires.

One approach for eliminating these disadvantages occurring from wires is to use wireless technologies such as wireless communication and wireless power transfer [5]. The utilization of wireless communication in robots enables sensors and actuators to be electrically separated and thus obviously resolves the wiring effort [6]. However, since this method requires wireless communication chips (ICs) and antennas on each node, a large footprint needs to be occupied, and moreover, a power source is needed to drive each e-skin component. Prior studies demonstrated selective driving of multiple actuators using a frequency selective inductive system [7], [8]. However, the required bandwidth correlates with the number of actuators; regulations and the general depletion of the spectrum strictly limit the number of modules this method can accommodate.

Another approach is to handle many slave modules via a common wired power bus. The communication using a power bus has been mainly researched in the context of power-line communication (PLC) [9]. Nevertheless, many of them are focused on large scales such as city-wide and house-wide equipment [10], while PLC has a huge potential in small devices including robots and wearable devices [11], [12]. In the context of wearable devices, a prior work proposed to simply input frequency-multiplexed analog signals into a pair of wires so the slave nodes can isolate the signal using bandpass filters [13], [14]. Although the slave modules can be selectively powered using this method, no communication channel for sensor feedback is established. Adoption of Code Division Multiple Access (CDMA) to power bus can realize the bi-directional communication between master and slaves [11]. Yet, CDMA requires rich modules for signal processing and the power consumption at each slave tends to be large. To reduce the power consumption, Noda, *et al.* utilized passive modulation to implement a frequency-multiplexed power bus inspired by I²C [15]. Instead of an ordinary I²C protocol that requires four lines (GND, VCC, SDA, and SCL), Noda, *et al.* enabled bi-directional communication and power delivery using a pair of wires and realized power bus using two sides of a textile. However, the modules can only talk one by one; a

Manuscript received: October, 14, 2019; Revised January, 12, 2020; Accepted March, 31, 2020. This paper was recommended for publication by Editor Cecilia Laschi upon evaluation of the Associate Editor and Reviewers’ comments. This work was supported by JST ERATO Grant Number JPMJER1501. The work of T. Sasatani was supported by JSPS Research Fellow program. (*Corresponding author: Yuki Nishizawa.*)

The authors are with The University of Tokyo, 7-3-1 Hongo, Bunkyo-ku, Tokyo, Japan nishizawa, sasatani, mishige, umedachi, kawahara@akg.t.u-tokyo.ac.jp, narusue@mlab.t.u-tokyo.ac.jp

Yuki Nishizawa is currently with Preferred Networks Inc., Otemachi Bldg., 1-6-1 Otemachi, Chiyoda-ku, Tokyo, Japan

Takuya Sasatani is also with JSPS Research Fellow program.

Takuya Umedachi is currently with Faculty of Textile Science and Technology, Shinshu University, 3-15-1 Tokida, Ueda-shi, Nagano, Japan

Digital Object Identifier (DOI): see top of this page.

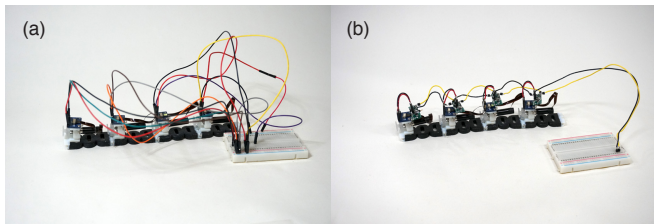


Fig. 1. Examples of wiring to the caterpillar-like robot, which has four actuators and four sensors. (a) Example of typical wiring. A Wire is required for each actuator/sensor. (b) Our proposed method, Ramus. Only two wires are required to connect all actuators/sensors; by utilizing frequency-multiplexing, we can selectively power actuators/sensors and also acquire sensor values simultaneously.

delay correlated with the number of slave modules occur, and this fluctuating delay makes this non-suitable for controlling multiple actuators based on sensor feedback.

To solve this issue, we propose Ramus: a frequency-multiplexed power bus integrated with up-link load-modulation communication. Load-modulation is a method that communicates by modulating the “reflection” of the incoming signals through changing the load impedance through a switch; the slave modules can modulate the reflection of incoming signals to send data to the master. Our proposed method is based on frequency multiplexing signals, therefore a small bandpass filter on the node is only needed to separate the uplink and downlink signals, whereas typical BUS communication such as I²C requires rich ICs to distinguish and embedded identification data. Moreover, our slave modules are designed to be frequency-selective (*i.e.*, receive signals only within a particular frequency band). Given that “*only the received signals can be reflected*” all slave modules can send sensor data at once, and the talking slave module can be determined from observing the frequency band in which the reflection occurred.

Our contributions are summarized as follows:

- 1) Proposal of a frequency-multiplexed power bus integrated with load-modulation communication. This enables real-time powering, controlling, and monitoring of many slave modules, via a power bus consisting of a single pair of wires without requiring ICs for digital signal processing at nodes.
- 2) A guideline to design the proposed power bus based on circuit analysis. Our analysis shows that eight channels can be accommodated within a 9 MHz frequency band.
- 3) A proof-of-concept demonstration of our method through driving a caterpillar-like robot that integrates sensor feedback.

II. PROPOSED METHOD

A. Frequency-Multiplexed Power Bus

A power bus distributes power from the source to the slave nodes using the shared bus lines. By adopting a power bus instead of standard one-to-one wiring, the number of wires can be reduced to only two. The overview of the system is shown in Fig. 2. The power bus is connected to the source

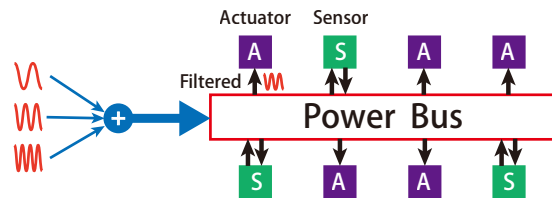


Fig. 2. Conceptual diagram of Ramus. Instead of wiring to each slave modules (actuator and sensor) one-by-one, we use a common “power bus”, which physically consists of two wires, to power, control, and monitor all slave modules.

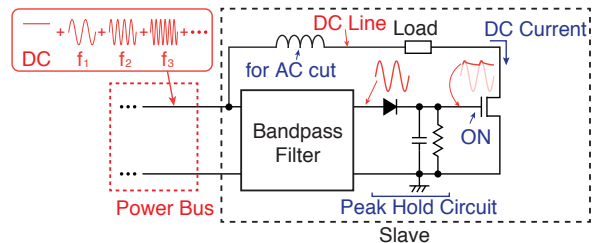


Fig. 3. Circuit diagram of the slave modules. Multiple sine waves (f_1, f_2, f_3, \dots) and a DC offset are superimposed at the input of the power bus. The DC filter (inductor) extracts DC power, which supplies power to the load of the slave module (*i.e.*, actuator, sensor, etc). The Bandpass filter selectively extracts a certain frequency signal (f_1 in the figure above) and inputs to the peak-hold circuit, which acquires the amplitude of frequency f_1 . This signal switches the ON/OFF state of the transistor, which controls the DC flowing into the load. Consequently, the load is supplied power when a signal of frequency f_1 is input to the power bus.

wave generator and slave nodes. The source wave generator multiplex multiple sine waves on different frequencies; each sine wave corresponds to the input of each slave node and controls the ON/OFF state of the load power supply. The output of the source is input to the power bus along with DC that is used to power the sensors and loads. We utilized coupling capacitors to superimpose signals onto DC bus [16]. The detailed block diagram of slave nodes is illustrated in Fig. 3. A slave node consists of a DC filter (*i.e.*, choke coil), a bandpass filter, and a load. The DC filter separates DC power from AC signals. The bandpass filter extracts a certain frequency signal from the power bus. If the signal in the power bus contains the particular frequency signal corresponding to the filter, the transistor turns on and enables the DC power supply to the load. Although the tested state is bi-modal, either ON or OFF, the control of output actuators using Pulse-Wave Modulation (PWM) waves is also possible in a similar way.

The details of the implemented circuit will be described in the next subsection.

B. Sensor Feedback System

Since robots integrate sensors to control themselves (*i.e.*, feedback control to reach target displacement, speed, etc), we need a method to obtain the sensor values from each slave node in addition to powering them. To read sensor values from each slave node without adding extra wires, each slave node needs

to communicate through the filters. If sensors use digital communication protocols such as I²C, those signals will be cut off by the bandpass filter and will not reach the master part. Meanwhile, adding ICs for signal processing requires not just additional space but also will increase power consumption, which are both not preferable in our application. As each sensor is allocated only a specific frequency band, sensors are required to communicate using this frequency band. To resolve these issues, we utilize load modulation [17]; we convert analog sensor value to a pulse with frequency f_s , which corresponds to the sensor value, and switch the load impedance using this pulse. The overview of our sensor feedback system is illustrated in Fig. 4. In this method, the resultant waveform becomes as illustrated in Fig. 5. By applying Fourier Transform to convert this waveform to the frequency domain, we obtain a spectrum as shown in Fig. 6. Since the operation of multiplying two waves corresponds to the convolution of a spectrum, two peaks appear on both sides of the f_c peak with a distance of f_s from the center.

Thus, the power source can obtain the switching frequency by reading the frequency distance between each center peak and side peaks. If sensor values are represented in pulses, as in encoders, the detected frequency represents the sensor value. For analog sensors, such as a current sensor, bending sensor, and temperature sensor, the output of sensors are often retrieved in voltage. In such cases, a voltage-controlled oscillator (VCO) could be used; VCO converts voltage input to pulse with a frequency corresponding to the voltage.

The range and precision of sensor value are described by characteristics of the standard fast Fourier transform (FFT) algorithm, that is:

$$\Delta f = \frac{f_{sample}}{n} \quad (1)$$

where n is the number of samples and f_{sample} is a sampling frequency of the waveform. Precision can be enhanced by either increasing n or decreasing f_{sample} .

To obtain the modulated signal, we use a directional coupler. A directional coupler can isolate the traveling wave and reflected wave from the transmission line, essentially for monitoring purposes. As the change of load impedance in load modulation appears as a change of reflected wave, the modulated signal can be detected by analyzing the reflected wave. In our implementation, the directional coupler is inserted between the signal generator and power bus, and the reflected wave is analyzed using a spectrum analyzer.

III. DESIGN AND IMPLEMENTATION

The essential components of Ramus are a bandpass filter, load modulation switch, and wave generation/spectrum detection hardware.

A. Bandpass Filter

The analog filters at each slave node have both DC filter and AC bandpass filter. DC power is filtered using 47 μ H inductor, and AC signals are filtered by bandpass filters

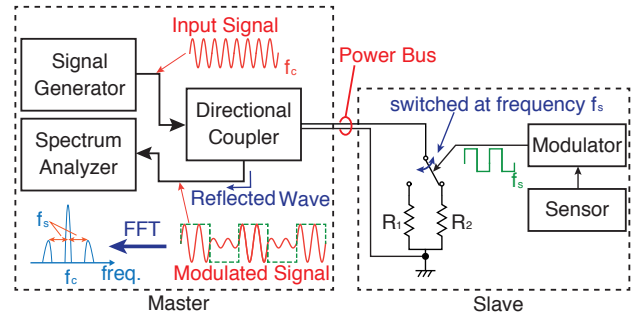


Fig. 4. Overview of the sensor feedback system. Our method retrieves the sensor value via load modulation communication; a carrier frequency f_c is input via the bandpass filter to the slave node, and the slave node switches between two loads (*i.e.*, R_1, R_2) at frequency f_s , which modulates the reflected wave; by setting f_s based on the sensor value, the sensor value can be sent back to the master. Finally, the master decodes sensor data from the frequency spectrum of the reflected wave.

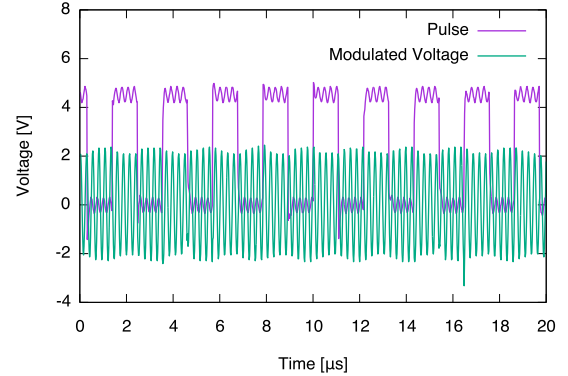


Fig. 5. The pulse waves generated from the voltage-controlled oscillator and the modulated signal. The modulated signal is the voltage measured at the switch in Fig. 4.

shown in Fig. 7. Because the frequency range that could be utilized is limited by the wave generator hardware and components, it is our challenge to narrow the bandwidth of each filter so that a larger number of actuators could be fit in the same range. Therefore, we regard the designing each bandpass filter is essential to adopt the power bus method to real applications.

Our bandpass filter uses series and parallel LC resonance filters combined to narrow the bandwidth. Here, the transfer function of our bandpass filter for voltage can be described using the following equation:

$$H_v(\omega) = \frac{V_2}{V_1} = \left[1 + \left(j\omega C_p + \frac{1}{j\omega L_p} \right) \left(j\omega L_s + \frac{1}{j\omega C_s} \right) + \frac{1}{R_{load}} \left(j\omega L_s + \frac{1}{j\omega C_s} \right) \right]^{-1}$$

where ω is an angular frequency ($=2\pi f$) of the AC voltage, R_{load} is the resistance of the load, L_s and C_s are the inductance and capacitance of LC series resonance filter, and

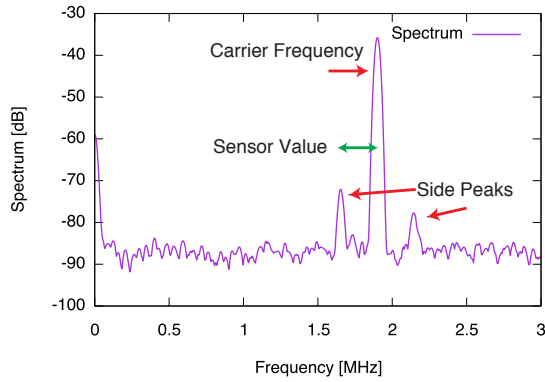


Fig. 6. A spectrum of the modulated signal in Fig. 5. The frequency peak in the center represents the carrier frequency f_c , and the modulated frequency appears as side peaks with a distance of f_s from the carrier frequency.

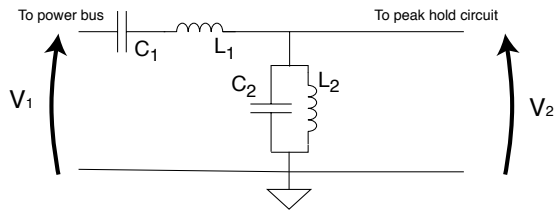


Fig. 7. Design of the bandpass filter. The proposed filter consists of a series LC bandpass filter and a parallel LC notch filter to keep the bandwidth narrow. Note that this model does not account for parasitic resistance/capacitance/inductance for simplicity.

L_p and C_p are those of parallel resonance filter. These filters have a resonance frequency at $\omega_0 = \frac{1}{\sqrt{L_s C_s}} = \frac{1}{\sqrt{L_p C_p}}$.

The objective of filter design is to have transfer functions that have the maximum peak at target frequency and low values at other frequencies. To design the optimal filter, we define the bandwidth of this filter as the width of the peak; that is, by defining ω_1 and ω_2 are the frequencies that voltage at the load drops to a half of the voltage at the target frequency ω_0 , the bandwidth $\Delta\omega$ equals to $|\omega_1 - \omega_2|$. Since in ideal filter $H_v(\omega_0) = 1$, $H_v(\omega_1)$ and $H_v(\omega_2)$ are $1/2$. By solving $H_v(\omega) = 1/2$ for ω , the bandwidth is calculated as follows:

$$\Delta\omega = \omega_0 \sqrt{\frac{-(\alpha^2 - 2k) + \sqrt{(\alpha^2 - 2k)^2 + 12k^2}}{2k^2}} \quad (2)$$

where $\alpha = \frac{\omega_0 L_s}{R_{load}}$, and $k = \frac{L_s}{L_p} = \frac{C_p}{C_s}$. From the Equation 2, it is concluded that increasing k decreases the bandwidth, and $\Delta\omega$ increases as ω_0 becomes higher. To keep the bandwidth constant over the whole frequency range, it is important to adopt higher k for higher target frequency ω_0 .

B. Load Modulation

Load modulation is implemented as switching the impedance of the load at a certain frequency corresponding to the sensor value. In our implementation, we tested a current sensor and photo reflector. Since both sensors have an

analog voltage output, we use VCO (LTC6990 from Linear Technology) to convert sensor values to frequency-modulated pulses.

Fig. 8 shows the change of pulse frequency when the current value changes. The current is controlled using a potentiometer (variable resistor) attached as a load and measured using source meter. The figure shows that the measured frequency is in a linear relationship with current, implying that current value can be successfully determined via the observation of frequency change. By fitting the parameter of the line prior to the measurement, the correct current value can be calculated. The current values at multiple potentiometers connected to a single bus are successfully observed as shown in Fig. 9.

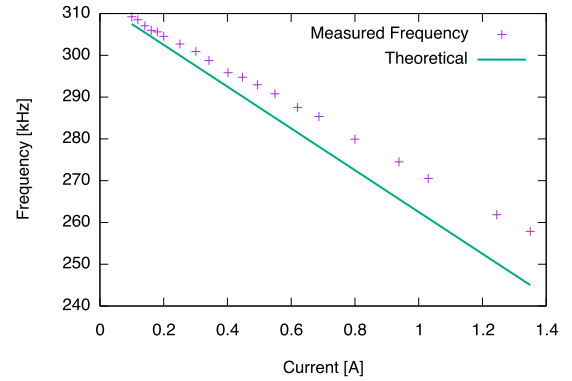


Fig. 8. Generated pulse frequency in response to the change of current. Although measured frequency slightly differs from the value calculated from the datasheet, we can see a linear relationship, implying that the current value can be calculated from the pulse frequency.

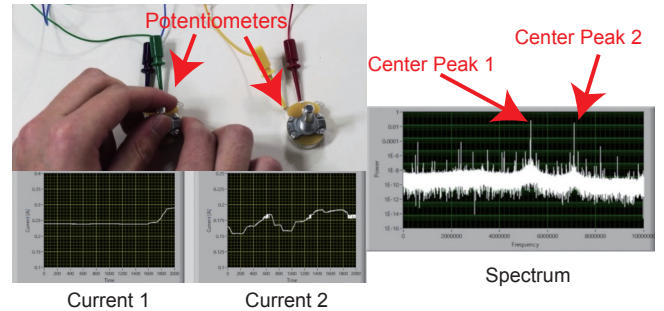


Fig. 9. Simultaneously receiving multiple sensor feedbacks. The figure shows the values of the current flowing two potentiometers (variable resistors) and the raw spectrum used for calculation. Two center peaks correspond to each potentiometer, and the current value is calculated using side peaks of each center peak.

C. Wave Generation and Spectrum Detection

As a wave generator is required to generate several frequency waves at the same time, we utilized Universal Software Radio Peripheral (USRP) for this role. USRP can multiplex arbitrary signals to certain frequency waves; for example, if a signal of 1 MHz sine wave is multiplexed to the wave of 10 MHz carrier frequency, the output signal becomes the convolution of these two waves, whose

frequency spectrum has peaks at $10 - 1 = 9$ MHz and $10 + 1 = 11$ MHz in addition to 10 MHz. If the signal of the sum of 1 MHz and 2 MHz is multiplexed, the five peaks appear at 8, 9, 10, 11, 12 MHz. Therefore, by choosing an appropriate carrier frequency and signals, USRP can generate waves consisting of arbitrary frequency waves.

The advantage of using USRP also includes that it can be used as a spectrum analyzer. By choosing a carrier frequency and bandwidth that are high enough to cover the analyzed frequency range, USRP can read the waveform of the modulated signals, and the frequency spectrum can be acquired by performing FFT on the observed waveform. Since both signal generator and spectrum analyzer features are concluded in USRP process, it is easy to integrate sensor feedback in real applications.

As mentioned in Section III-A, the filter bandwidth, and the sensor feedback mechanism should be carefully considered to fully utilize the frequency-multiplexed power bus. Let us consider the case where we can use a spectrum up to 9 MHz. We configured the voltage-controlled oscillator so that the upper bound of the output frequency is 500 kHz, therefore, each carrier should be separated by at least 1 MHz. Thus, we can accommodate eight channels (*i.e.*, carriers) in this frequency range.

The carrier frequencies start from 1.5 MHz with intervals of 1 MHz; the channel at the highest frequency is at 8.5 MHz. Note that these frequencies should be selected so that the interference between each other is minimized. One major cause of interference likely to occur in naively designed systems is harmonics and the frequency error of the USRP, which lead to cross-talk (*i.e.*, signal leakage to other carriers). Harmonics occur when the sine-waves are slightly distorted and the system contains non-linear components (*e.g.*, diodes, transistors); the effect of harmonics can be alleviated by simply setting the carrier frequencies so that no carrier is an integer multiple of other carriers. We simply make the first three digits of frequency prime numbers here for this. Cross-talk is interference caused by signal leakage from one channel adjacent ones. To avoid this phenomenon, we designed the target frequencies not to be multiples of 1 MHz.

As explained in Equation 2, to keep the filter bandwidth constant, it is important to control k . Considering the relationship between inductance and bandwidth, we chose high-quality inductors shown in Table I for filter implementation. These values are also confirmed using the circuit simulation (assuming a 50-ohm power amplifier). The voltage transfer function of each filter is shown in Fig. 10. Although the peak voltage drops as frequency increases, the bandwidth is constant, and interference between channels is successfully prevented. The voltage drop is a result of adopting low-inductance inductors as L_p ; thus there is a trade-off between narrowness of a band and its peak voltage. If the number of slave nodes is smaller, we can use larger inductors L_p which makes the interval larger.

IV. APPLICATION

We demonstrate how Ramus can be used in robotic applications by driving a caterpillar-like robot shown in

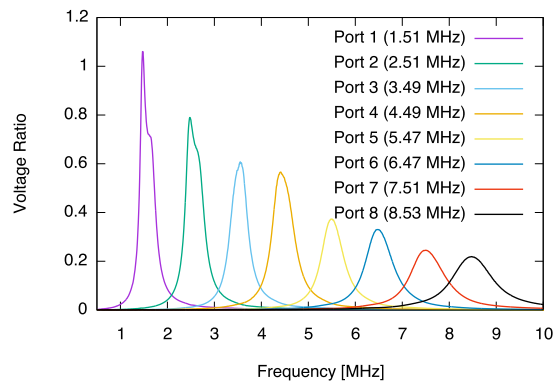


Fig. 10. The measured transfer function for each slave node. We can see that the channels are successfully separated from each other; which enables the independent driving of multiple actuators.

Fig. 12 [18]. It is required that the actuators in this robot is synchronized and has an offset at a certain phase to proceed; therefore, individual control of the actuators, as well as feedback from each actuator, is mandatory.

The black parts are made of a rubber-like material, and the body can extend and contract along the body axis. The robot consists of four segments, and each segment is equipped with a small motor and the boards of Ramus. Each segment has a string that penetrates the segment; when the motor winds this string, the segment shrinks. The filter board filters selectively extract the frequency component corresponding to itself and control each motor. The sensor board has a current sensor (ACS70331 from Allegro Microsystems) to measure the current flowing the motor; this current value indicates whether a segment is shrunk as shown in Fig. 11. As explained in Section III-B, we obtain this current value by observing the modulated frequency of a pulse signal as the frequency gap of the side peak. A segment is regarded as shrunk when the frequency exceeds a threshold. Once a segment is shrunk, a motor on the next segment is actuated to contract it. This results in the locomotion of the robot.

In this application, we have a 9 MHz frequency range for four actuators; thus, we can take the frequency interval between the filters larger than 1 MHz. We have chosen 1.9, 2.9, 4.7, 7.1 MHz as target frequencies.

Fig. 13 shows the actuation of our robot. The segment shrinks from back to front, propelling the body forward.

V. DISCUSSION

A. Maximum Number of Channels

Our power bus can utilize as many channels as instruments and components allow, since regulations for radio waves do not apply to our wired system. Due to the limited communication bandwidth between the USRP

TABLE I
INDUCTORS USED IN FILTER

Freq. [MHz]	1.51	2.51	3.49	4.49	5.47	6.47	7.51	8.53
L_s [μ H]	22	22	22	22	22	22	22	22
L_p [nH]	470	240	100	100	68	68	68	68

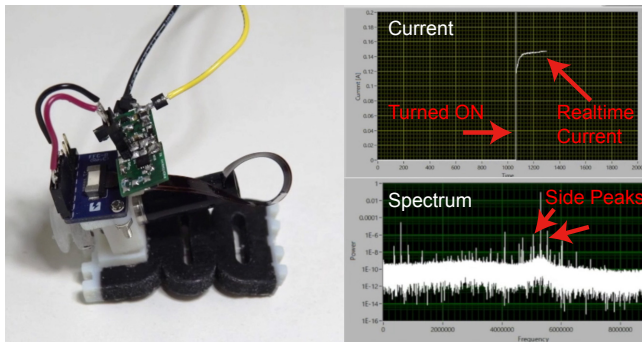


Fig. 11. Shrink of each segment can be detected using the current sensor, as motor current increases with torque rise. The value of the current sensor was calibrated before measurement.

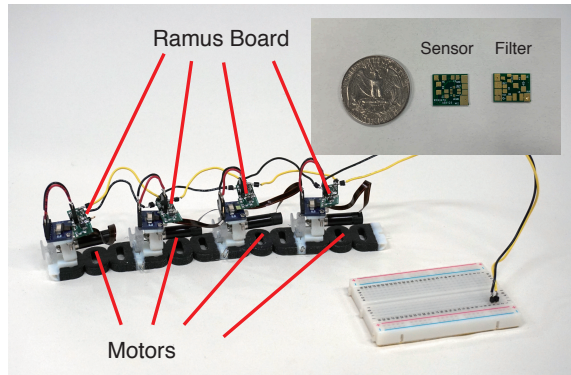


Fig. 12. Driving a caterpillar-like robot using AlvuS. The body consists of four segments, and each segment has a motor and a sensor/filter board, which drives the motor and sends back sensor data.

(USRP-2944R) and the computer (we used LabVIEW to control USRP), our current setup could only utilize the frequency range from DC to 15 MHz. However, additional engineering effort (e.g. implementation on an FPGA, integration of multiple USRPs, and a computer with SFP+ board installed) would mitigate this limitation. Also, it is possible to scan the spectrum multiple times with different carrier frequencies to utilize an even wider range.

Another bottleneck for increasing channels is the efficiency and self-resonant frequencies (SRF) of small components such as capacitors and inductors. Typical chip inductors of high inductance (over 1 μH) have SRF at 10 to 100 MHz and are not usable beyond this range. Although other low-inductance or low-Q inductors are available at such high frequencies, they cause wide bandwidth and low efficiency after all.

B. Interference between Channels

Our master node currently conducts FFT and reads the connected sensor values through the frequency of the side peaks. Therefore, external noises might interfere with this value. Although the peaks are distinguishable without using any complex protocols in our application, integrating techniques used in existing protocols (e.g., error correction) may enhance the fidelity of communication, which we consider as a possible future research direction.

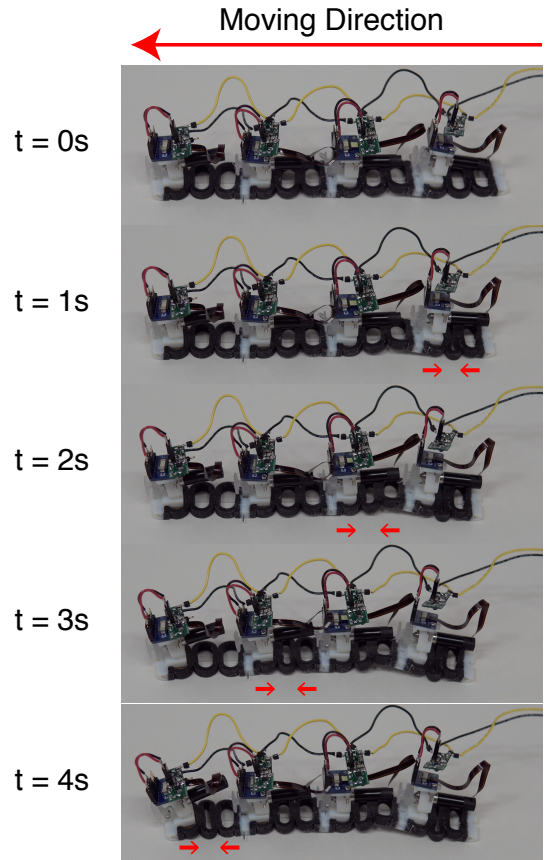


Fig. 13. The gait of the caterpillar-like robot. Each segment shrinks in turn based on the sensed current values at each motor. Ramus takes care of selectively controlling each segment and retrieving the sensed current values from each segment to enable feedback-based control.

In this paper, we aimed to control 10 actuators/sensors using 10 MHz bandwidth, which means each channel is allocated on a 1 MHz frequency band. To avoid interference with adjacent channels, we set the output frequency of the VCO to range up to 500 kHz. Although we have not seen critical interference between adjacent channels in this setup, it is also possible to configure VCO to the lower frequency so that interference becomes less likely to occur by sacrificing the precision.

C. Real-time Sensing

Although our power bus system can retrieve the sensor feedback almost in real-time, its precision depends on FFT parameters. As shown in Equation 1, precision can be increased by taking more samples; however, considering that taking n samples of sampling frequency f_{sample} requires $\frac{n}{f_{\text{sample}}} = \frac{1}{\Delta f}$ seconds, this affects the real-time sensor retrieval.

D. Size Reduction

Our filter uses combinations of typical capacitors and inductors; therefore, by selecting components carefully, the size of boards could be made even smaller. Also, our sensor board utilizes VCO and a current sensor that are

commercially available; by integrating them in a single chip, its size is expected to become dramatically smaller.

VI. CONCLUSION

We utilized Ramus, a sensor-feedback enabled frequency-multiplexed power bus, in small robots to realize transmission of power and signals to many slave nodes only using two cords. We have integrated the load modulation to a power bus, enabling sensor feedback control of the robots without adding extra wires. Our filter designing method enabled eight channels in 9 MHz frequency range, and successfully feedback-controlled a caterpillar-like robot.

ACKNOWLEDGEMENT

I would like to thank Kazunobu Sumiya for providing us with neat illustrations and Ken Takaki for helping us implement the robots. This work was supported by JST ERATO Grant Number JPMJER1501.

REFERENCES

- [1] Q. He, Z. Wang, Y. Wang, A. Minori, M. T. Tolley, and S. Cai, "Electrically controlled liquid crystal elastomer-based soft tubular actuator with multimodal actuation," *Science Advances*, vol. 5, no. 10, 2019. [Online]. Available: <https://advances.sciencemag.org/content/5/10/eaax5746>
- [2] S. Kim, C. Laschi, and B. Trimmer, "Soft robotics: a bioinspired evolution in robotics," *Trends in Biotechnology*, vol. 31, no. 5, pp. 287–294, 2013.
- [3] K. Y. Ma, P. Chirarattananon, S. B. Fuller, and R. J. Wood, "Controlled flight of a biologically inspired, insect-scale robot," *Science*, vol. 340, no. 6132, pp. 603–607, 2013.
- [4] S. Felton, M. Tolley, E. Demaine, D. Rus, and R. Wood, "A method for building self-folding machines," *Science*, vol. 345, no. 6197, pp. 644–646, 2014.
- [5] A. Kurs, A. Karalis, R. Moffatt, J. D. Joannopoulos, P. Fisher, and M. Soljačić, "Wireless power transfer via strongly coupled magnetic resonances," *Science*, vol. 317, no. 5834, pp. 83–86, 2007. [Online]. Available: <http://science.sciencemag.org/content/317/5834/83>
- [6] J. Byun, Y. Lee, J. Yoon, B. Lee, E. Oh, S. Chung, T. Lee, K.-J. Cho, J. Kim, and Y. Hong, "Electronic skins for soft, compact, reversible assembly of wirelessly activated fully soft robots," *Science Robotics*, vol. 3, no. 18, 2018. [Online]. Available: <https://robotics.sciencemag.org/content/3/18/eaas9020>
- [7] M. Boyvat, J.-S. Koh, and R. J. Wood, "Addressable wireless actuation for multijoint folding robots and devices," *Science Robotics*, vol. 2, no. 8, p. eaan1544, 2017.
- [8] K. Zhu, H. Nii, O. N. N. Fernando, and A. D. Cheok, "Selective inductive powering system for paper computing," in *Proceedings of the 8th International Conference on Advances in Computer Entertainment Technology*, ser. ACE '11. New York, NY, USA: ACM, 2011, pp. 59:1–59:7. [Online]. Available: <http://doi.acm.org/10.1145/2071423.2071497>
- [9] M. S. Yousuf and M. El-Shafei, "Power line communications: An overview - part i," in *2007 Innovations in Information Technologies (IIT)*, Nov 2007, pp. 218–222.
- [10] G. Bumiller, L. Lampe, and H. Hrasnica, "Power line communication networks for large-scale control and automation systems," *IEEE Communications Magazine*, vol. 48, no. 4, pp. 106–113, April 2010.
- [11] Chun-Hung Liu, E. Wade, and H. H. Asada, "Reduced-cable smart motors using dc power line communication," in *Proceedings 2001 ICRA. IEEE International Conference on Robotics and Automation (Cat. No.01CH37164)*, vol. 4, May 2001, pp. 3831–3838 vol.4.
- [12] E. Wade and H. H. Asada, "Wearable dc powerline communication network using conductive fabrics," in *IEEE International Conference on Robotics and Automation, 2004. Proceedings. ICRA '04. 2004*, vol. 4, April 2004, pp. 4085–4090 Vol.4.
- [13] Y. Tajima, A. Noda, and H. Shinoda, "Signal and power transfer to actuators distributed on conductive fabric sheet for wearable tactile display," in *International AsiaHaptics conference*. Springer, 2016, pp. 163–169.
- [14] A. Noda and H. Shinoda, "Frequency-division-multiplexed signal and power transfer for wearable devices networked via conductive embroideries on a cloth," in *Microwave Symposium (IMS), 2017 IEEE MTT-S International*. IEEE, 2017, pp. 537–540.
- [15] A. Noda and H. Shinoda, "Inter-ic for wearables (i2we): Power and data transfer over double-sided conductive textile," *IEEE Transactions on Biomedical Circuits and Systems*, vol. 13, no. 1, pp. 80–90, Feb 2019.
- [16] E. Wade and H. H. Asada, "Cable-free wearable sensor system using a dc powerline body network in a conductive fabric vest," in *The 26th Annual International Conference of the IEEE Engineering in Medicine and Biology Society*, vol. 2, Sept 2004, pp. 5376–5379.
- [17] K. Finkeneller, *RFID handbook: fundamentals and applications in contactless smart cards, radio frequency identification and near-field communication*. John Wiley & Sons, 2010.
- [18] T. Umedachi, M. Shimizu, and Y. Kawahara, "Caterpillar-inspired crawling robot using both compression and bending deformations," *IEEE Robotics and Automation Letters*, vol. 4, no. 2, pp. 670–676, April 2019.